Atmospheric Forcing of Dust Source Activation across East Asia

Chen et al.

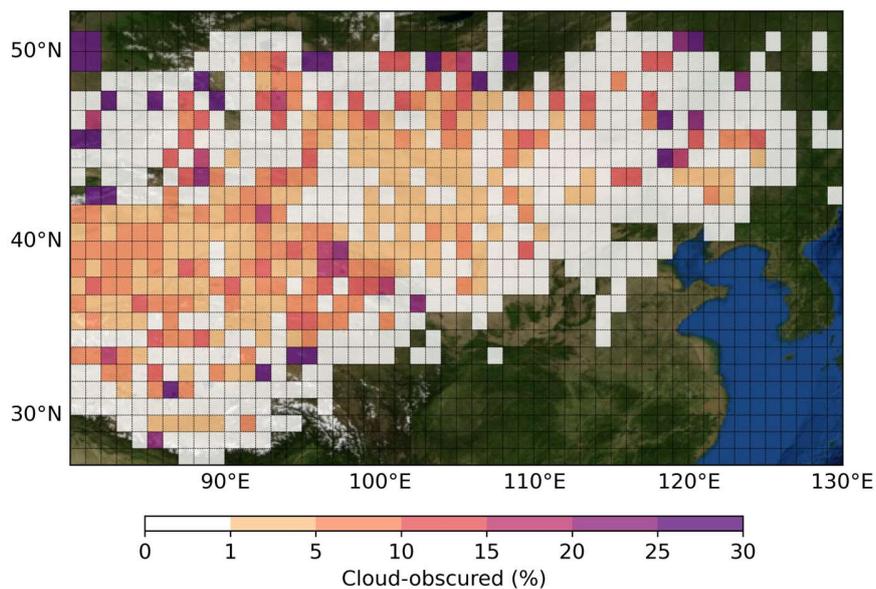*Correspondence to:* Lingle Chen (lingle.chen@soton.ac.uk)

Figure S1. Spatial distribution of the proportion of cloud-obscured dust source activation (DSA) across East Asia. Colours show the percentage of all DSA records within each 1° × 1° grid cell that were classified as cloud-obscured, i.e. cases in which dust activation events may have occurred but could not be confidently identified due to cloud cover and are therefore not included in the main DSA statistics. Basemap from NASA's Blue Marble: Shaded Relief imagery © NASA.
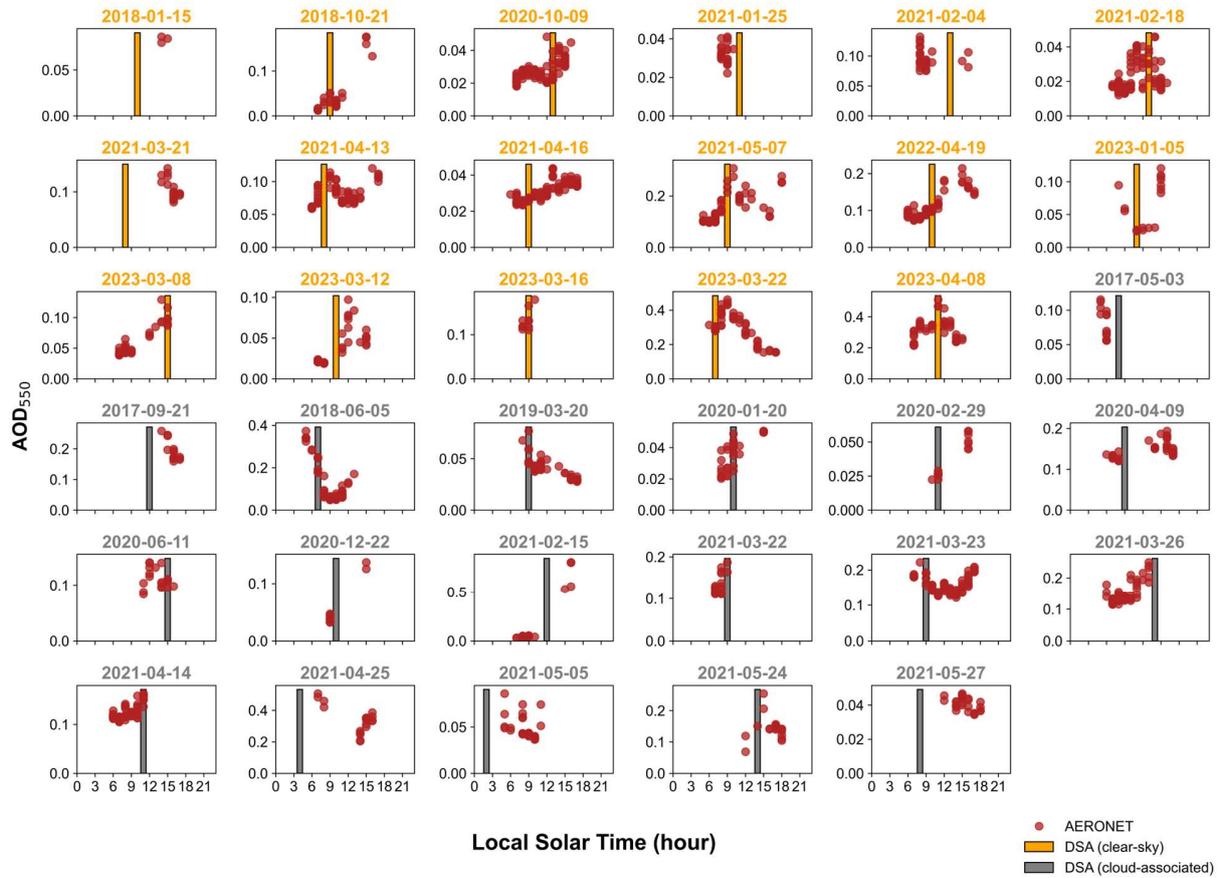
Figure S2. Cross-comparison between daily aerosol optical depth (AOD$_{550}$; dots) from the AERONET site at Dalanzadgad (43.577°N, 104.419°E) and the timing of Himawari-8/9 detections of dust source activation (DSA; bars) within the corresponding grid cell (43–44°N, 104–105°E) under clear-sky (orange) and cloud-associated (grey) conditions. Each panel represents one dusty day among all available cases from 2016 to 2023 when AERONET observations and DSA events were simultaneously available for the Dalanzadgad grid. AOD$_{550}$ represents the column-integrated atmospheric dust loading. The figure highlights the reproducibility of DSA timing relative to the AOD$_{550}$ peaks, given that AOD$_{550}$ may include contributions from dust transported from other sites and data gaps.
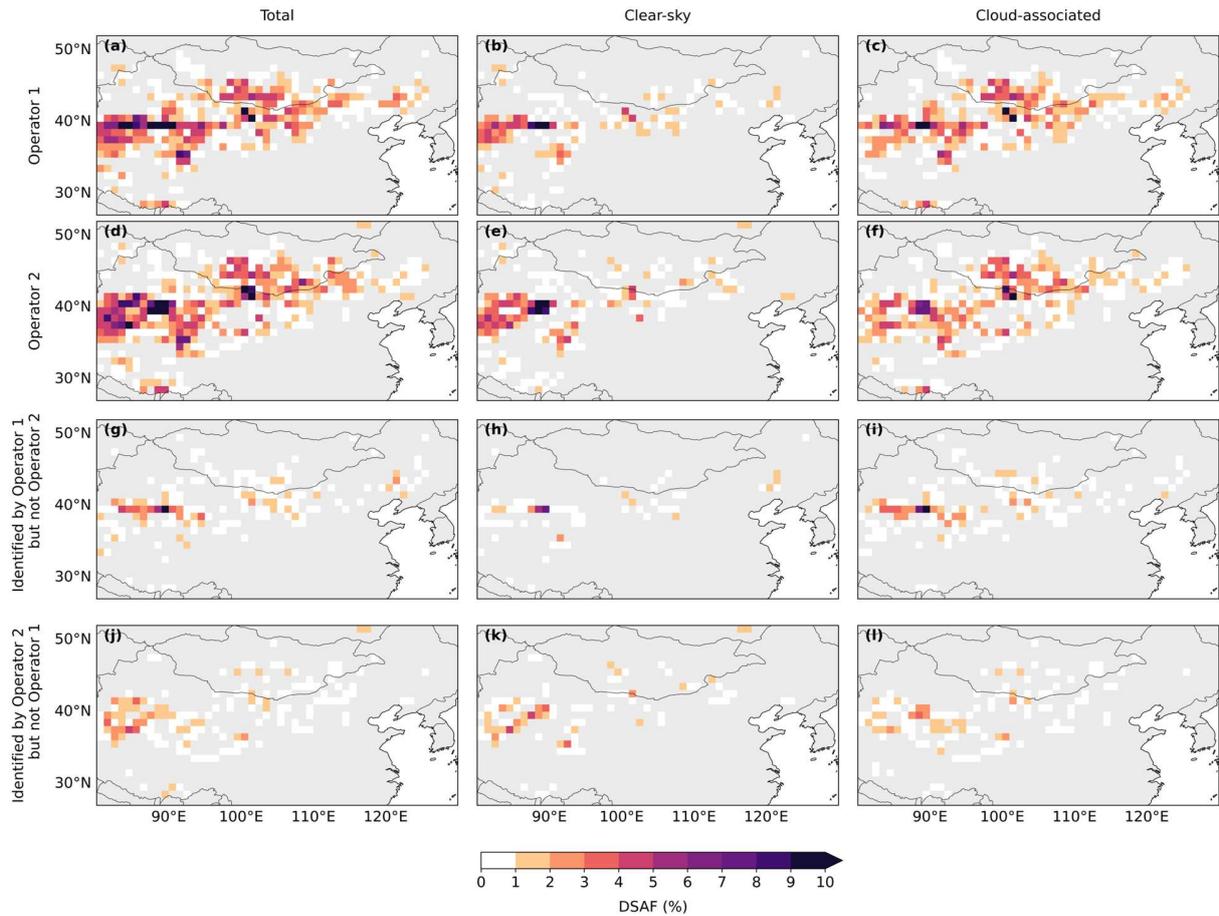
Figure S3. Inter-operator comparison of dust source activation frequency (DSAF, %) derived independently by two operators over four months of data randomly distributed throughout the study interval. Columns show total (clear-sky + cloud-associated), clear-sky, and cloud-associated dust activation; rows show (a-c) Operator 1, (d-f) Operator 2, (g-i) events identified by Operator 1 but not Operator 2, and (j-l) events identified by Operator 2 but not Operator 1. The bottom two panels indicate grid cells where dust source activation events were not matched by the other operator within a ±1 h temporal and ±1° spatial tolerance. DSAF mismatch in the Taklimakan Desert can be explained by dust activation obscured by cloud cover and by complex basin-scale floating dust.
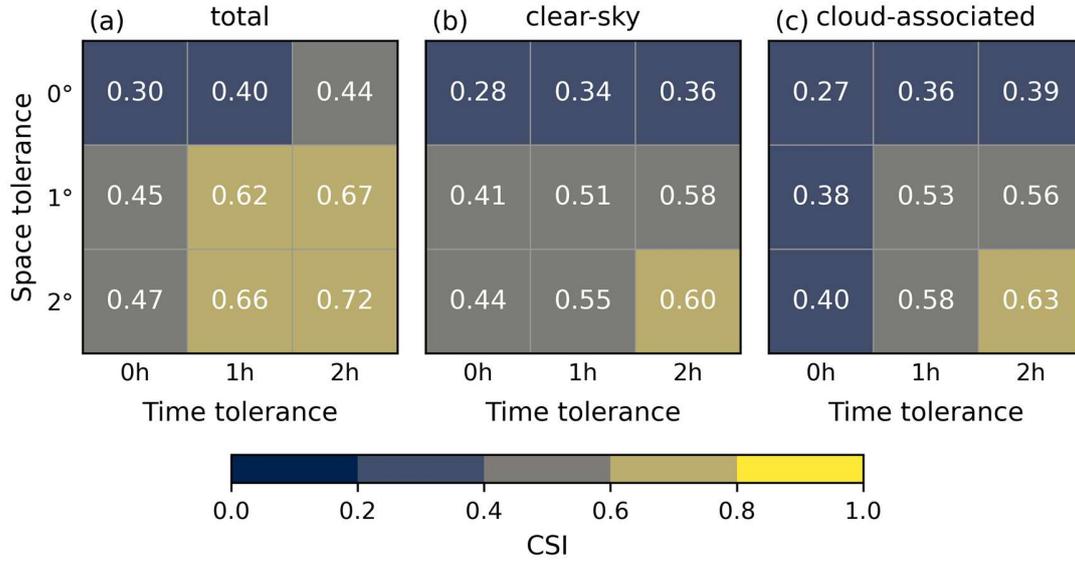
Figure S4. Critical Success Index (CSI) analysis based on a relabelled four-month dataset produced independently by two labellers. CSI values are shown for (a) total dust events, (b) clear-sky events, and (c) cloud-associated events, evaluated across combinations of temporal (0–2 h) and spatial (0–2°) tolerances. The CSI quantifies the level of agreement between the two independently generated labelling datasets and is defined as

$$\text{CSI} = \frac{I}{C + K - I},$$

where I denotes the number of matched events, and C and K denote the total number of events identified independently by each labeller. CSI ranges from 0 (no agreement) to 1 (perfect agreement).
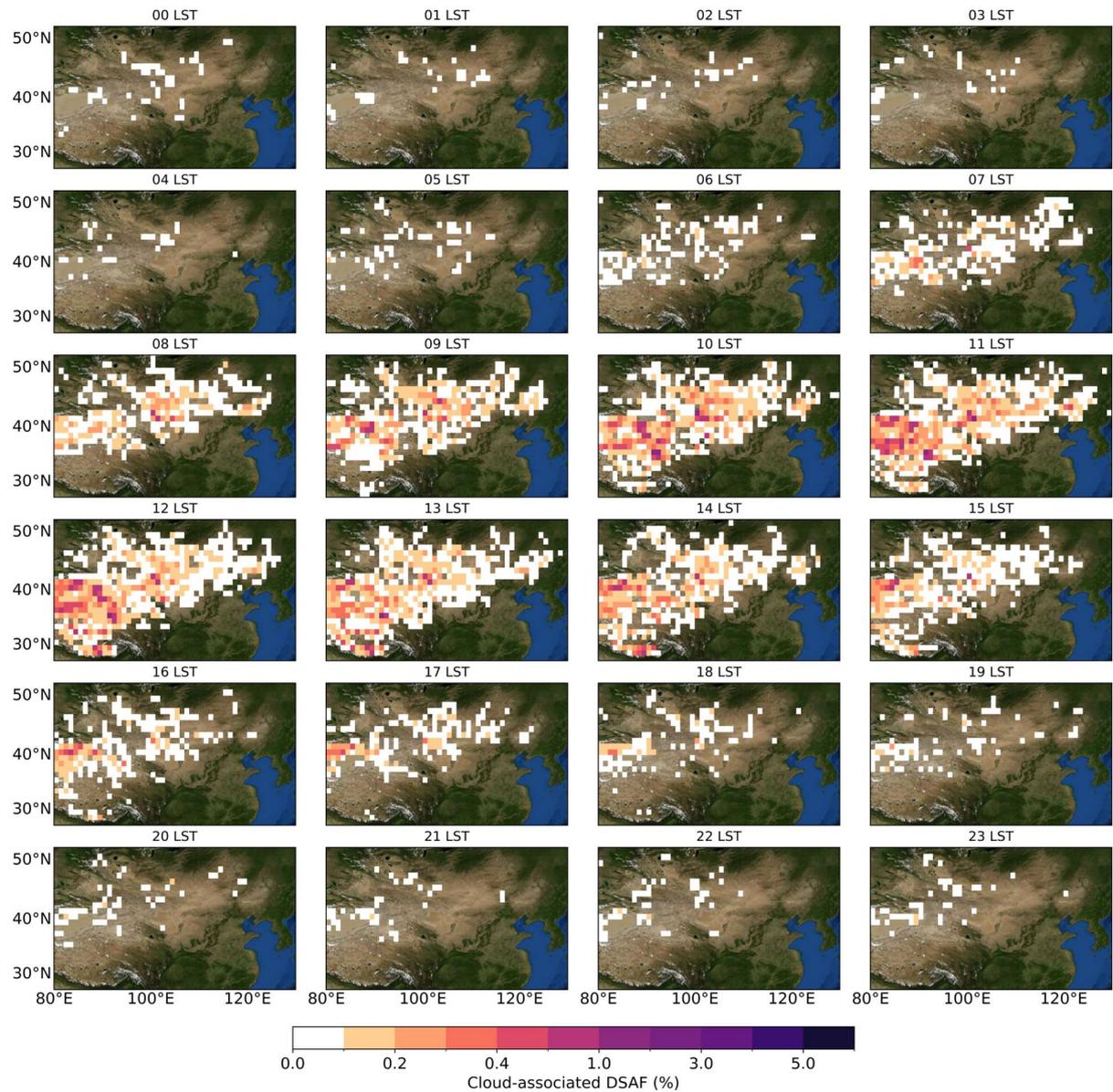
Figure S5. Average annual dust source activation frequency (DSAF) in East Asia from 2016 to 2023 under cloud-associated conditions for all hours between 00:00 and 23:00 local solar time (LST). Basemap from NASA's Blue Marble: Shaded Relief imagery © NASA.
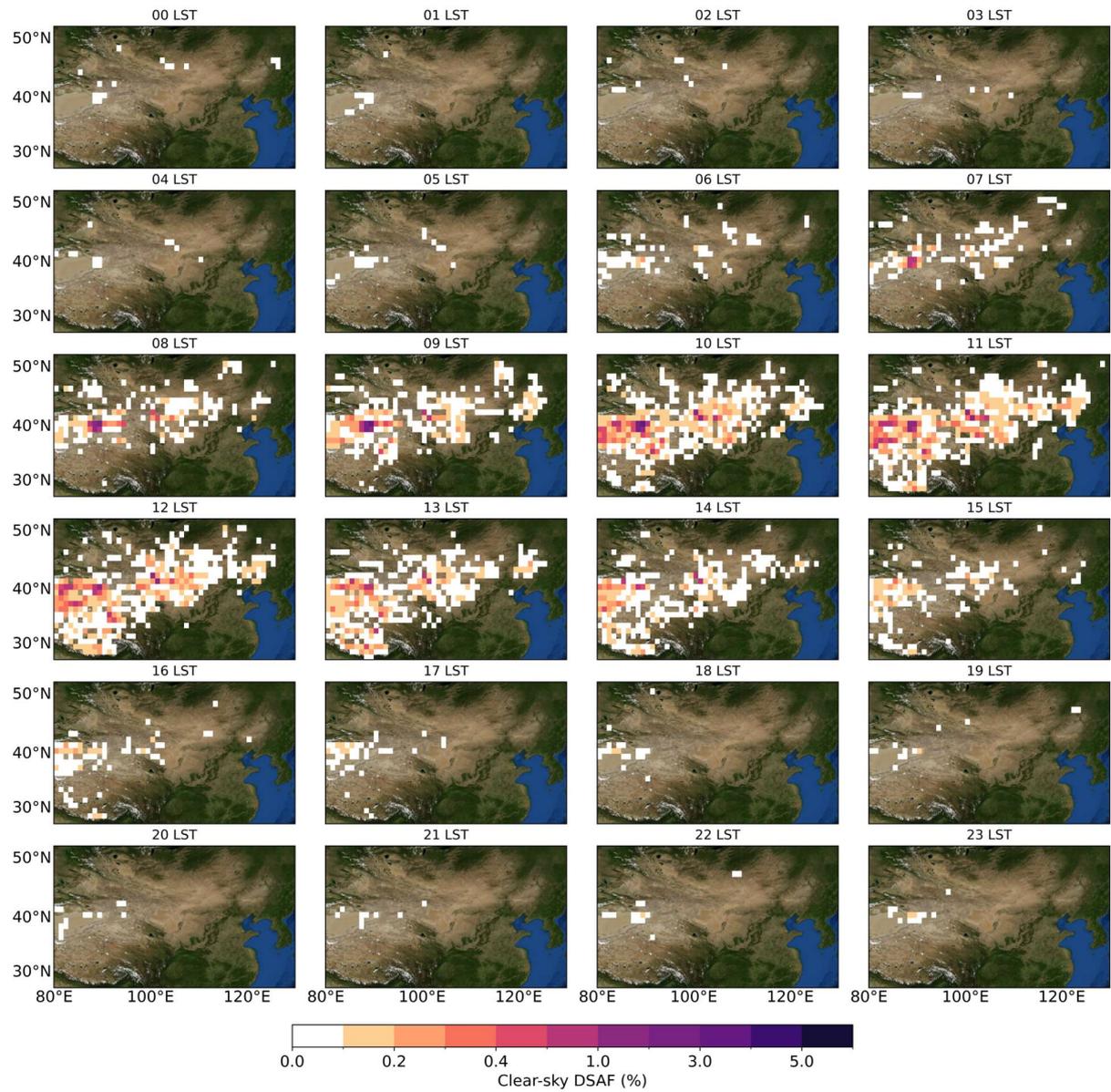
Figure S6. Average annual dust source activation frequency (DSAF) in East Asia from 2016 to 2023 under clear sky conditions for all hours between 00:00 and 23:00 local solar time (LST). Basemap from NASA's Blue Marble: Shaded Relief imagery © NASA.
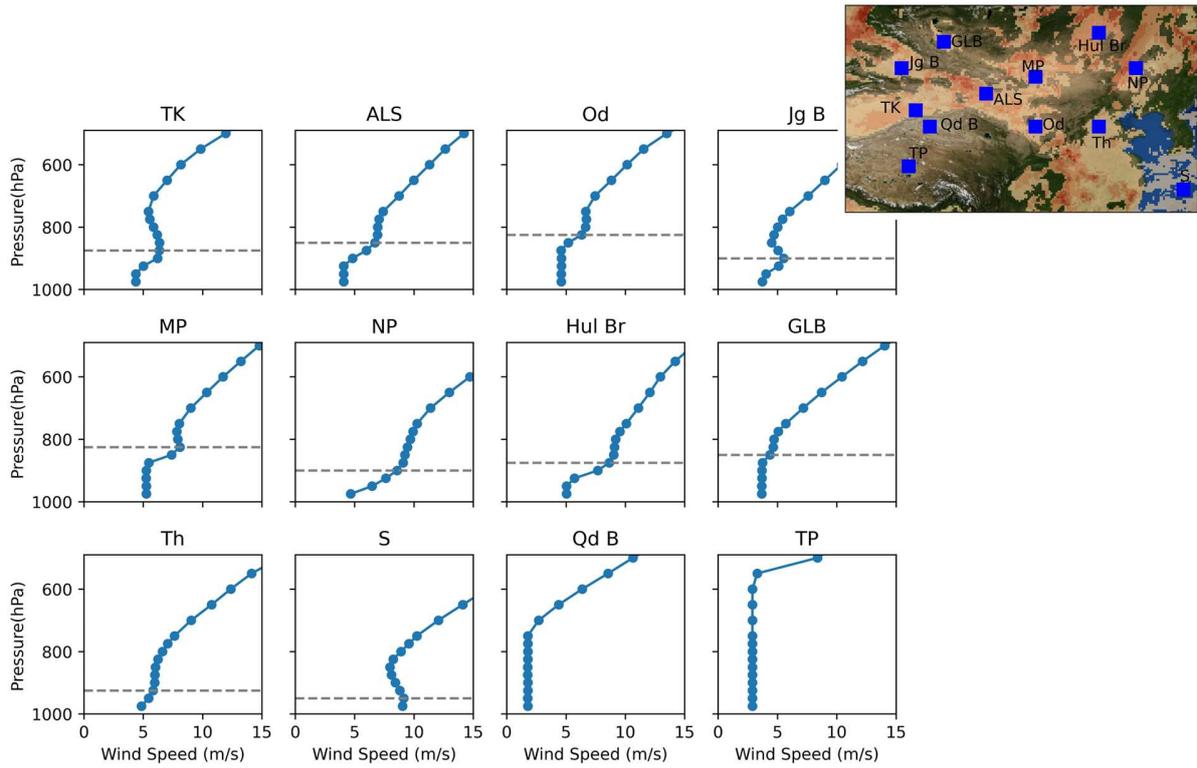
Figure S7. Wind profiles averaged over 2016–2023 for selected regions used to determine the jet-nose height. The grey dashed lines indicate the jet nose height characterized by a wind speed maximum. High LLJ occurrence regions labelled in black include the Taklimakan Desert (TK), the Alashan Plateau (ALS), the Ordos Plateau (Od), the Junggar Basin (Jg B), the Mongolian Plateau (MP), the Northeast Plain (NP), the Hulun Buir Desert (HL), the Great Lake Basin (GLB), the east side of Taihang Mountain (Th), the China East Sea (S), the Qaidam Basin (Qd B), and the Tibetan Plateau (TP). Inset basemap from NASA's Blue Marble: Shaded Relief imagery © NASA.
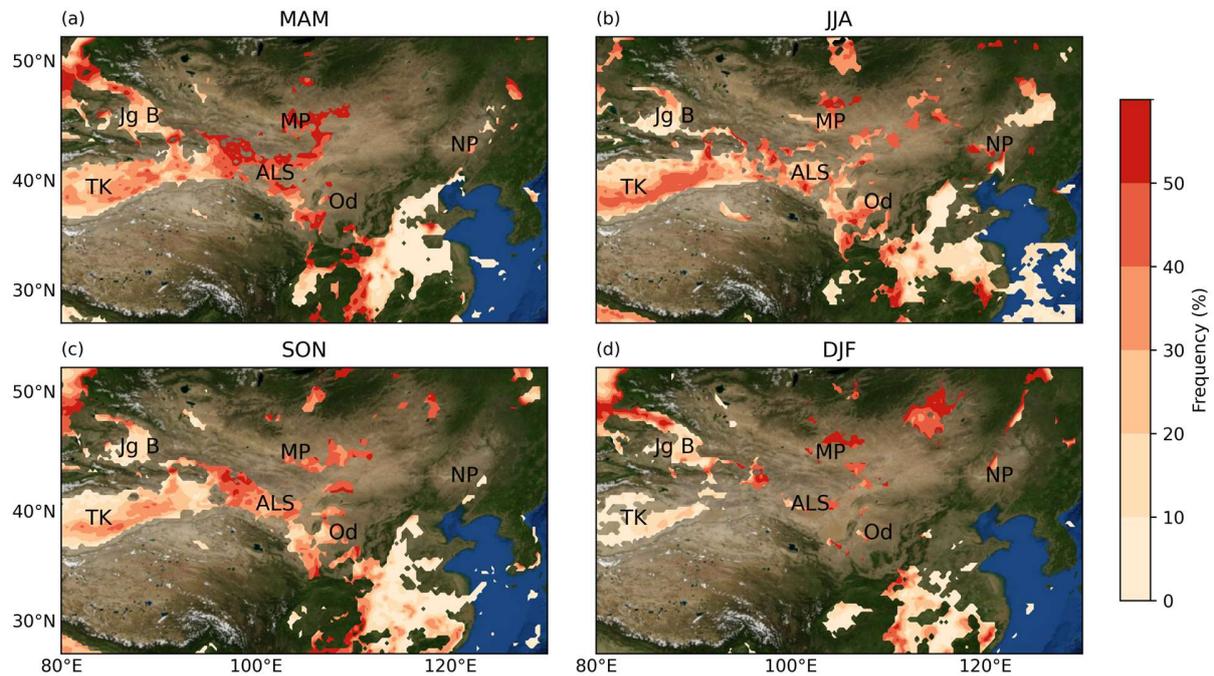
Figure S8. Seasonal frequency (%) of low-level jet (LLJ) occurrence. For each grid cell, LLJ frequency is calculated as the number of days on which the wind-speed difference (Δv) between the 975 hPa level and the jet-nose pressure is ≥ 5 m s^{-1} at 06:00 local solar time (LST), divided by the total number of days in the corresponding season across 2016–2023. Seasons are: (a) Spring (March–May; MAM), (b) Summer (June–August; JJA), (c) Autumn (September–November; SON), and (d) Winter (December–February; DJF). Regions of high LLJ occurrence (black labels) include the Junggar Basin (Jg B), the Mongolian Plateau (MP), the Alashan Plateau (ALS), the Northeast Plain (NP), the Taklimakan Desert (TK), and the Ordos Plateau (Od). Basemap from NASA's Blue Marble: Shaded Relief imagery © NASA.
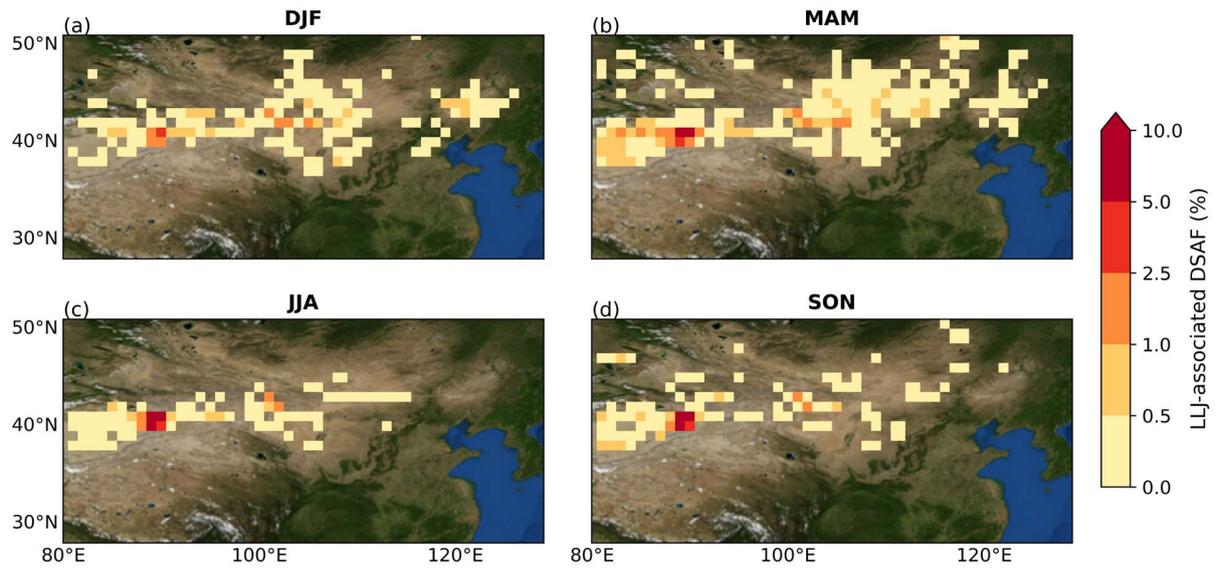
Figure S9. Seasonal low-level jet (LLJ)-associated dust source activation frequency (DSAF) across East Asia (2016–2023). LLJ-associated DSAF is defined as the percentage of observation days with clear-sky dust source activation between 09:00 and 12:00 local solar time (LST) coincident with LLJ occurrence at 06:00 LST, normalized by seasonal observation days. Panels show seasonal means for (a) spring (March–May, MAM), (b) summer (June–August, JJA), (c) autumn (September–November, SON), and (d) winter (December–February, DJF).